Clays and Clay Minerals, Vol. 66, No. 1, 1–8, 2018.

THE FORMATION OF Fe-BEARING SECONDARY PHASE MINERALS FROM THE BASALT–SEDIMENT INTERFACE, SOUTH PACIFIC GYRE: IODP EXPEDITION 329

KIHO YANG[1], HANBEOM PARK[1], HIONSUCK BAIK[2], TOSHIHIRO KOGURE[3], AND JINWOOK KIM[1,*]

[1] Department of Earth System Sciences, Yonsei University, Sinchon-dong, Seodaemun-gu, Seoul 120-749, Korea
[2] Division of Analytical Research, Korea Basic Science Institute (KBSI), 74 Inchon-ro, Sungbuk-gu, Seoul 136-713, Korea
[3] Department of Earth and Planetary Sciences, Graduate School of Science, University of Tokyo 7-3-1 Hongo, Bunkyo-ku, Tokyo 113-0033, Japan

Abstract—Alteration of basalt is a ubiquitous process on the vast oceanic crust surface and results in the formation of secondary-phase minerals that include clay minerals and Fe-(oxyhydr)oxides. Thus, this process is a significant consequence of water/rock interactions that could reveal the (bio)geochemical conditions of formation. Core samples at the basalt/sediment interface from a depth of 74.79 m below sea floor (mbsf) were recovered during the International Ocean Discovery Program (IODP) expedition 329 (2010.10.10–2010.12.13) in the South Pacific Gyre (SPG). Two distinct regions of yellow- and red-colored sediment were observed. The mineralogy, elemental composition, Fe oxidation state, and mineral structure of the altered basalt samples were analyzed using transmission electron microscopy (TEM) with selected area electron diffraction (SAED) patterns, energy dispersive spectroscopy (EDS), electron energy loss spectroscopy (EELS), and micro X-ray fluorescence (μ-XRF). In the yellow sediment, K-nontronite and feroxyhyte (δ'-FeO(OH)) were the dominant mineral phases, while Mg-rich smectite (saponite), chlorite, and hematite were found predominantly in the reddish sediment. The appearance of K-nontronite and feroxyhyte mineral assemblages in altered sediment indicated that oxidative conditions prevailed during basalt alteration. Variation in the Fe-oxidation states in the K-nontronite structure, however, may indicate that local reducing conditions persisted throughout the biogeochemical reactions.

Key Words—Basalt Alteration, EELS, K-nontronite, Saponite, South Pacific Gyre.

INTRODUCTION

The formation of clay minerals and Fe-(oxyhydr)-oxides during the alteration of basaltic crust is a ubiquitous process over the vast surface of oceanic crust. The basalt alteration partially influences the composition of seawater (Hart and Staudigel, 1982), sources of Fe and P for microorganisms (Orcutt *et al*., 2011) and Fe cycling (Roden and Zachara, 1996). Fe-rich smectites, such as nontronite, have been discovered on hydrothermally-altered basalt surfaces (Cuadros *et al.*, 2008; Dekov *et al*., 2008; Cuadros *et al*., 2013), and a proto-type of smectite was found in deep sea sediments under low temperature conditions in the South Pacific (Cuadros *et al*., 2011). The alteration of basalt during interactions with the surrounding seawater through the hydration and dissolution of basaltic components results in smectite formation (Alt, 1995, 2009; Clayton and Pearce, 2000; Knowles *et al*., 2012). Moreover, K-nontronite has been identified in samples of Cretaceous basalt from the Caribbean Sea and Mid-Ocean Ridge basalt, which suggests oxidative weathering of basalt. This observation is important because K-nontronite could represent an intermediate process of smectite alteration (Melson and Thompson, 1973); however, the mechanism of K-nontronite formation in natural sediments is not well understood, especially concerning the role of microbes in K-nontronite formation (Koo *et al*., 2014).

Fe-(oxyhydr)oxides form as a secondary mineral in basaltic crust (Edwards *et al*., 2005; Knowles *et al*., 2012) and often coexist with clay minerals under oxidative conditions at low temperatures (Bach and Edwards, 2003). Fe-(oxyhydr)oxides are a significant source of Fe for organisms and act as terminal electron acceptors in the electron transport chain to gain energy for growth and metabolism (Nealson and Saffarini, 1994). Fe bioavailability in a marine environment is strongly influenced by mineral species and particle size (Cornell and Schwertmann, 2003; Glasauer *et al*., 2003), which indicates possible basalt alteration by microbes (Fisk *et al*., 2003). Nevertheless, most basalt alterations have been reported as abiotic processes.

Microbes can reduce structural Fe in clay minerals (Stucki *et al*., 1987; Wu *et al*., 1988). Local variations in the redox states of Fe in nontronite can be associated with the oxidation of surrounding organic matter (Eslinger *et al*., 1979) or localized microbial Fe-respiration (Gates *et al*., 1998; Kim *et al*., 2003, 2004; Stucki and Kostka, 2006; Dong *et al*., 2009; Jaisi *et al.*, 2011; Koo *et al*.,

* E-mail address of corresponding author:
jinwook@yonsei.ac.kr
DOI: 10.1346/CCMN.2018.064083

This paper was originally presented during the 3rd Asian Clay Conference, November 2016, in Guangzhou, China

2014). Thus, an investigation of the local variations in the oxidation states of Fe in smectite structures will to some extent enhance an understanding of the formation mechanisms and redox conditions in the biotic basalt reaction (Yang *et al*., 2016). Nanoscale measurements of the Fe-redox states in clay mineral structures by utilizing electron energy loss spectroscopy (EELS) are, therefore, necessary.

In the present study, altered basalt fragments with a sediment interface were recovered from the South Pacific Gyre (SPG) during IODP expedition 329. The oxidative conditions for the entire sedimentation history have persisted until the present due to the low sedimentation rates (<1.6−1.9 m/Myr), which cause an extremely low influx of terrestrial sediments, low bioproduction, and is called an "oligotrophic open ocean environment" (Glasby, 1991; Claustre and Maritorena, 2003; D'Hondt *et al*., 2009). Spectroscopy and microscopy measurements were made on the altered basalt area to determine the formation mechanism for secondary phase minerals, especially the nanoscale Fe-redox states in K-nontronite and to understand the biotic or abiotic K-nontronite formation conditions during basaltic crust alteration.

MATERIALS AND METHODS

Samples

Core samples of the basalt/sediment interface at a depth of 74.79 m below the seafloor (mbsf) were recovered at site U1365 (23º51.0493′S, 165º38.6624′W), SPG, during IODP expedition 329 (2010.10.10−2010.12.13). Thick sediments of pelagic clays and chert (total 75 m) overlay the oceanic basalt (~120 Ma; (D'Hondt *et al*., 2013; Yang *et al*., 2016)). The interface between the basaltic basement and sediments was highly disturbed and consisted of a mixture of altered basalt fragments and black-colored metalliferous pelagic sediments (D'Hondt *et al*., 2013). Samples (altered basalt fragments) were impregnated with low-viscosity L.R. White resin (acryl resin, Ted Pella, Inc., Redding, California, USA) (Kim *et al*., 1995), which penetrates the fractures or pores in a sample and maintains the original structure. A basalt slab was prepared and polished using Al_2O_3 powder (600 mesh) for micro X-ray fluorescence (μ-XRF) observations. Altered basalt samples from the yellow and red altered fractures on the basalt slab (Figure 1) were collected in 1.5-mL Eppendorf® tubes filled with deionized water and were subsequently dispersed using an ultrasonic bath. Samples were then gently dropped onto the surface of a C mesh-supported transmission electron microscopy (TEM) Cu-grid for TEM and EELS measurements.

Micro X-ray fluorescence (μ-XRF)

The μ-XRF analysis was performed using a Bruker M4 Tornado μ-XRF analyzer (Bruker, Karlsruhe, Germany) with a Mo anode tube at Yonsei University. The X-ray (Mo) source was operated at 50 kV and 200 μA and interactions with the sample lasted for 1 s per scanning point. The distribution and amounts (wt.%) of K, Fe, and Si were measured *via* a two-dimensional area scan. Point-scanned elemental compositions (wt.%) of Fe, Ca, Si, Al, Mg, K, Ti, and Mn were measured to identify distinctively altered areas (see arrows in Figure 1). The absolute errors for the μ-XRF quantifications (wt.%) were approximately <0.1% for Na, Mg, Al, K, Ca, and Fe and 0.4% for Si.

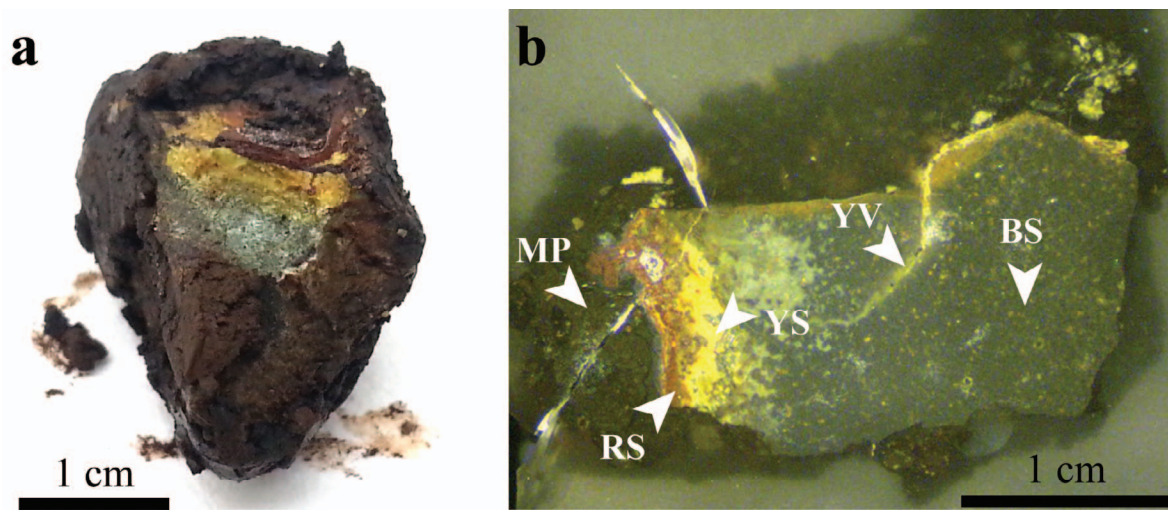

Figure 1. Optical photographs of altered basalt samples that display a) altered basalt fragment in the red/brown-colored metalliferous pelagic sediments and b) thin-sectioned L.R. White resin-embedded samples. Arrows indicate the altered areas that distinctively show metalliferous pelagic sediments (MP), red altered sediments (RS), yellow altered sediments (YS), yellow vein (YV), and basalt substrate (BS).

https://doi.org/10.1346/CCMN.2018.064083 Published online by Cambridge University Press

Transmission electron microscopy (TEM) and electron energy loss spectroscopy (EELS)

Lattice fringes, selected area electron diffraction (SAED) patterns, and energy dispersive spectroscopy (EDS) analyses of the structural and elemental compositions of the clay minerals were obtained using a JEOL JEM-2010 UHR TEM operated at 200 kV and equipped with a JEOL JED-2200 EDS (JEOL, Tokyo, Japan) at the University of Tokyo, Japan. The redox states of the Fe in the clay structures were quantified as a function of the integral ratio of EELS spectra for Fe-L_3/L_2 (van Aken and Liebscher, 2002). The EELS measurements were performed at the Korea Basic Science Institute (KBSI) using a FEI Technai G^2 F30 ST EF-TEM (FEI Company, Hillsboro, Oregon, USA) equipped with a Gatan Imaging Filter (GIF) operated at 300 kV. The operational settings for EELS data acquisition were entrance aperture of 2.0 mm, energy dispersion of 0.2 eV/channel, convergence angle of 0.5 mrad, collection angle of 20.0 mrad, and full width at half-maximum (FWHM) for the zero-loss peak (ZLP) calibration at 1.0 eV. The EELS spectra exposure times were 0.01 s and the total acquisition time in the scanning TEM (STEM) mode lasted 5.0 s. For each sample, a total of 500 EELS spectra signals were collected and summed. The background signal was removed from the EELS spectra and the Fe-L_3/L_2 integral ratios were measured using the standard power-law and double arctan background function (van Aken and Liebscher, 2002; Yang *et al*., 2016) using the Gatan Digital Micrograph (Gatan Inc., Pleasanton, California, USA) software program.

RESULTS

Texture of altered basalt and elemental distribution

The optical micrograph of a resin-impregnated altered basalt (Figure 1) has five distinct altered areas indicated by different colors and textures. Metalliferous pelagic sediments (MP) overlie the altered basalt fragment, which consists of red altered sediments (RS), yellow altered sediments (YS), and a yellow vein (YV). Yellow pits (~ 0.2 mm in diameter) are widely distributed on the light-gray basalt substrate (BS) and the yellow vein extends into the yellow altered sediments.

The variations in elemental composition of the MP, RS, YS, YV, and BS altered areas were measured using μ-XRF (Figure 2) and the results are summarized in Table 1. The elemental Ca, K, Fe, and Si distributions had drastic variations that depended on the particular

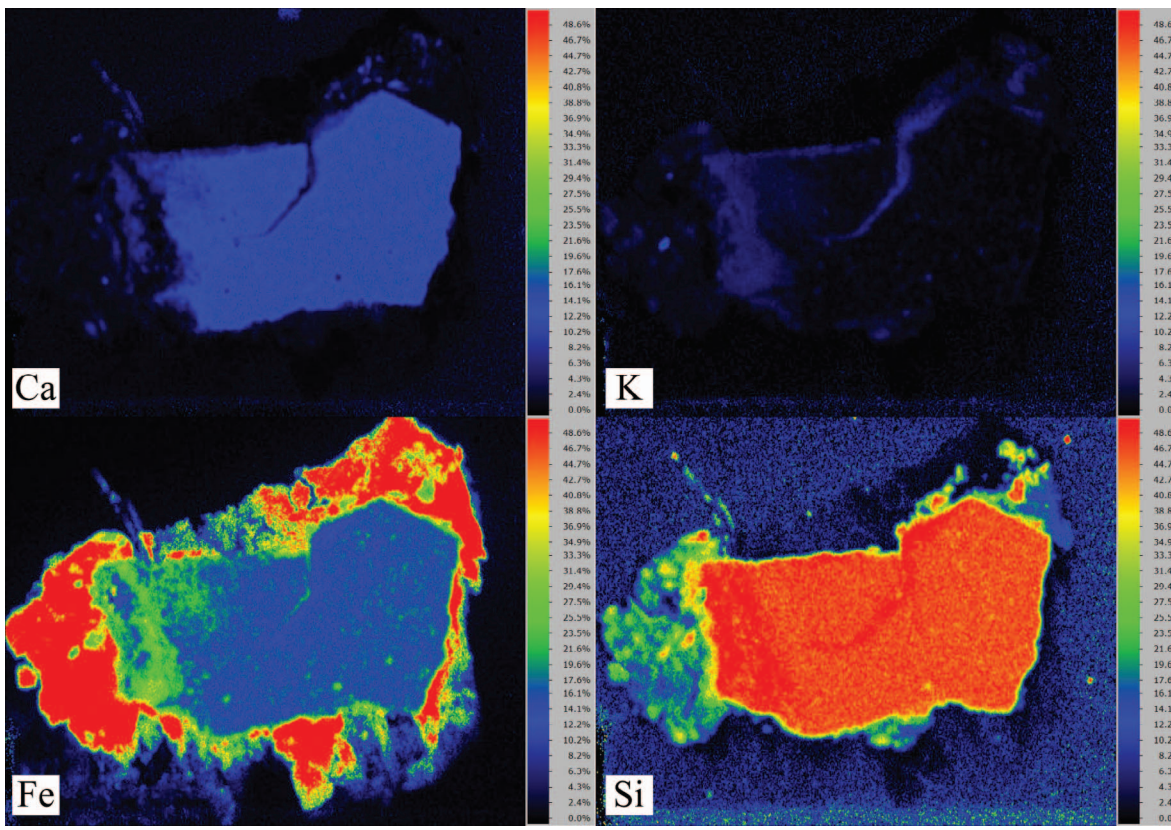

Figure 2. Two-dimensional elemental Ca, K, Fe, and Si distribution maps of the altered basalt fragment measured using micro X-ray fluorescence (μ-XRF). The elemental concentrations (wt.%) are indicated by the color index at the left of each illustration. The concentrations decrease in the order red>yellow>green>blue (white>black for grayscale).

https://doi.org/10.1346/CCMN.2018.064083 Published online by Cambridge University Press

Table 1. Micro X-ray fluorescence (μ-XRF) elemental distributions (wt.%) in altered basalt samples in comparison to a fresh, tholeiitic basalt (Zhang *et al.*, 2012).

	Metalliferous pelagic sediments	Red altered sediment	Yellow altered sediment	Yellow vein	Basalt substrate	Fresh basalt (Zhang *et al.*, 2012)
Fe	74.68	27.46	39.18	23.13	27.27	10.22
Ca	1.21	9.33	2.77	8.06	17.49	12.32
Si	11.42	40.95	37.32	40.82	38.86	49.50
Al	1.51	10.32	6.47	11.68	10.29	15.32
Mg	3.36	5.57	3.72	5.38	1.82	7.43
K	1.10	4.07	6.27	7.93	1.29	0.07
Ti	0.35	2.12	4.22	2.73	2.58	1.45
Mn	6.36	0.18	0.05	0.28	0.41	0.14

altered area. For example, the Ca contents in the altered YS, YV, and RS areas were 2.77−9.33% in comparison to 17.49% in the basalt BS; the measured K contents in RS (4.07%), YS (6.27%), and YV (7.93%) were higher than in BS (1.29%); the Fe contents in MP (74.68%) and YS (39.18%) were greater in comparison to the other areas (23.13−27.46%); but the Si contents were 37.32−40.95% in most areas, except MP. The concentrations of other elements, such as Mg and Al, were high, particularly in RS (5.57% and 10.32%) and YV (5.38% and 11.68%), but variations in the minor components, Ti and Mn, were only 2.12−4.22% and 0.05−0.41%, except MP.

TEM observations

Representative TEM bright-field micrographs for the secondary phase minerals displayed lattice fringes with insets to show the corresponding EDS plots and SAED patterns (Figures 3 and 4). A clay mineral phase with a 1.0-nm spacing in YS had defect-free, parallel, side-by-side packets (~70-nm thick each) with diffuse Bragg reflections (Figure 3a). The elemental composition of the 1.0-nm phase (Figure 3a) had an Al/Si ratio of 0.2 and high Fe and K contents, which is typical of a K-bearing, Fe-rich smectite. In the RS area, lattice fringes with wavy and layer-terminated structures had 1.0-nm spacings (Figure 3b) and thick, defect-free packets with 1.4-nm spacings (Figure 3c). The elemental composition of the 1.0-nm phase (Figure 3c) had a high content of Mg with an Al/Si ratio of 0.14, which is typical of a Mg-rich smectite. In contrast, the 1.4-nm phase had high Mg and Fe contents and an Al/Si ratio of 0.46, which is typical of chlorite. Aggregates of nanometer size particles (~10 nm in diameter) had randomly oriented crystals with 0.25-nm (Figure 4a) and 0.27-nm spacings (Figure 4b). The SAED patterns (Figures 4a, 4b) had discrete Bragg reflections, which are typical of δ'-FeO(OH) (0.13, 0.15, 0.17, 0.22, and 0.25 nm) and α-Fe_2O_3 (0.15, 0.17, 0.25, and 0.27 nm), respectively. The EDS plots (Figures 4a, 4b) had high Fe contents and confirmed the presence of Fe-(oxyhydr)-oxides.

Redox states of Fe

The EELS spectra of the secondary phase minerals in the YS and RS areas were quantified based on the universal curve (van Aken and Liebscher, 2002) as a function of the integral intensities of the Fe-L_3/L_2 peaks and the Fe(III) concentrations (Figure 5a). The accuracy of the estimated Fe(III) concentrations was tested by comparison to the integral intensity ratios of Fe-L_3/L_2 in well-characterized standards, such as bioreduced nontronite (NAu-1; 77.8% Fe(III), L_3/L_2 = 6.82; Koo *et al.*, 2014) and annite (49% Fe(III), L_3/L_2 = 5.18; Cape *et al.*, 1986) as shown in Figure 5b. This resulted in a good match with the measurements by van Aken and Liebscher (2002). The Fe-L_3 and Fe-L_2 edges appeared at 709 and 722 eV, respectively, and the integral intensities of Fe-L_3 and Fe-L_2 (gray colored areas) were calculated by using the background-removed EELS spectra (solid line) and the double arctan background function (dotted line) and setting the 2-eV energy windows (Figure 5a). The EELS quantification for the K-bearing, Fe-rich smectite (YS) had an Fe-L_3/L_2 integral intensity ratio of 3.21, which matches the Fe(III) concentration of 35%. These values were comparable to previously measured Fe(III) concentrations for the Fe-rich smectite and the K-bearing, collapsed, Fe-rich smectite that were detected in the MP area (Yang *et al.*, 2016; Figure 5a). Moreover, the Fe-(oxyhydr)oxides in the RS area hematite had an Fe(III) concentration of 100% and an Fe L_3/L_2 integral intensity of 9.58.

DISCUSSION

Secondary phase minerals

Optical observations of the RS and YS basalt interfaces and the YV vein (Figure 1) clearly indicated altered regions and a basalt/water interaction. The elemental distribution indicated that Ca was depleted and K, Mg, Fe, and Si were enriched (Figure 2 and Table 1).. Furthermore, the palely mottled BS area had yellow pits and high K and Fe contents in comparison to fresh tholeiitic basalt (U1365E-2R-1-W 65/69) collected

https://doi.org/10.1346/CCMN.2018.064083 Published online by Cambridge University Press

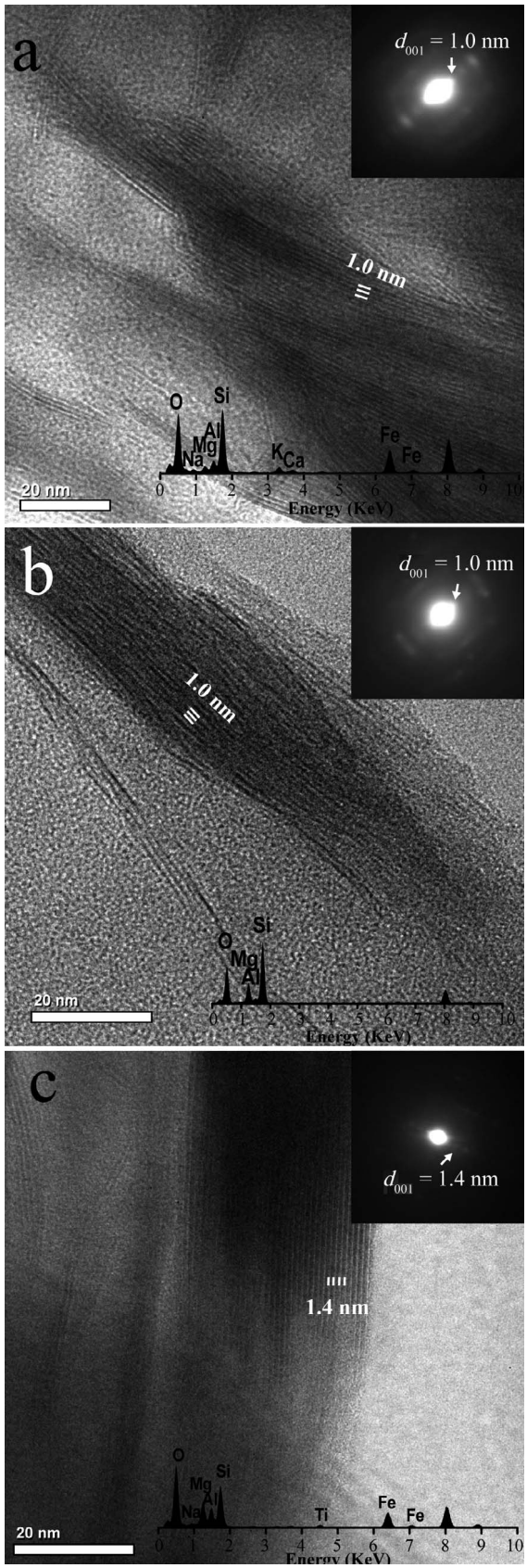

from the deeper basalt core (71 mbsf to 124.2 mbsf) at the same drilling site (Zhang *et al*., 2012). This suggests that the basalt fragment interface with sediments (Figure 1) is altered by interactions with seawater at a low temperature (Clayton and Pearce, 2000; Orcutt *et al*., 2013). Moreover, the formation of a K-bearing, Fe-rich smectite in the YS area clearly explains K and Fe enrichment during basalt alteration. The likely mechanism of K uptake is diffusive exchange with seawater (Clayton and Pearce, 2000). The formation of feroxyhyte and hematite in the altered basalt (RS and YS areas) was attributed to the significant amount of Fe-(oxyhydr)-oxides in the MP sediments, which suggests this is the origin of the red-brown to yellow-brown semiopaque oxide mineral (RSO) described by Yang *et al.* (2016). The YS and RS area color differences are associated with the different mineral assemblages and reflect variations in K and Fe contents. The Fe-(oxyhydr)oxide is dominant in the RS area, whereas a mixture of secondary phyllosilicate and Fe-(oxyhydr)oxide precipitates are dominant in the YS area (Pichler *et al*., 1999). A distinct zonation was observed in the YS area of the inner part and the basalt characteristics of the outer rim of the RS area indicates a progressive inward alteration process. The abiotic Fe oxidation and Fe-(oxyhydr)oxide precipitation on the surface of the basaltic substrate occurred by interactions with oxygenized seawater, whereas the K-rich secondary phyllosilicates formed during non-oxidative diagenesis in the fractures and pits of the basaltic substrate (Bass, 1976; Seyfried *et al*., 1978). Nonetheless, the process of replacement was not clearly understood by Pichler *et al*. (1999) nor particularly by Alt *et al*. (1995, 2009) for the biotic alteration of basalt.

K-nontronite

The K-bearing, Fe-rich smectites (K-nontronite) frequently observed at sediment/basalt interfaces is explained by the hydrothermal alteration of basaltic glasses in a submarine environment (Melson and Thompson, 1973) and by the replenishment of K and O through diffusive exchange with seawater during oxidative alteration (Clayton and Pearce, 2000). In the present study, the EELS measured structural Fe oxidation states in smectite (Figure 5) suggest that K-nontronite possibly forms by K uptake and by an Fe-rich smectite (nontronite) redox reaction. The K-nontronite and the characteristic Fe redox states are important in under-

Figure 3. Bright-field transmission electron microscopy (TEM) micrographs of representative clay mineral phases with lattice fringes and corresponding insets for energy dispersive spectroscopy (EDS) and selected area electron diffraction (SAED) patterns for a) K-bearing collapsed Fe-rich smectite in the yellow altered sediments (YS), b) Mg-rich smectite in red altered sediments (RS), and c) chlorite in RS.

https://doi.org/10.1346/CCMN.2018.064083 Published online by Cambridge University Press

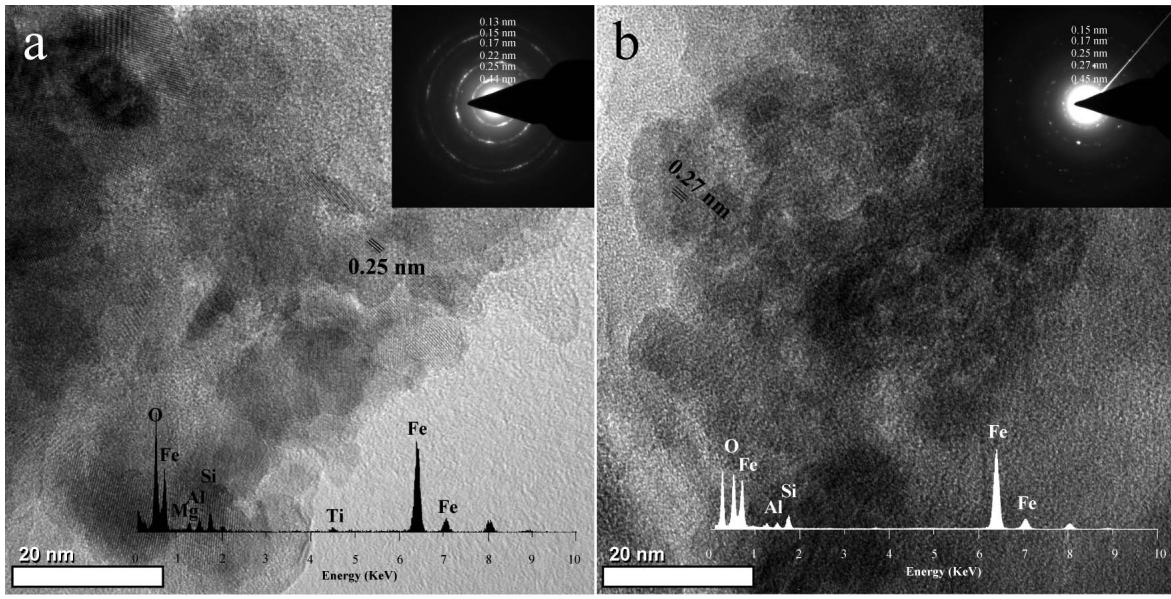

Figure 4. Bright-field TEM micrographs of a) feroxyhyte (δ′-Fe(III)O(OH)) in yellow altered sediments (YS) and b) hematite (α-Fe_2O_3) in red altered sediments (RS) with lattice fringes and corresponding insets for energy dispersive spectroscopy (EDS) and selected area electron diffraction (SAED) patterns. Randomly oriented nanosize particles (~10 nm in diameter) were observed.

standing the origin. Moreover, a K-nontronite formation mechanism was explained by Koo *et al*. (2014). Both nontronite and K-nontronite were observed in the MP sediment at the basalt/sediment interface (Yang *et al*., 2016). It is imperative to note that K-nontronite has more ferrous Fe (47% Fe(III) in MP and 35% Fe(III) in YS) than nontronite, which has more ferric Fe (78% Fe(III) in MP) as shown in Figure 5. Other examples of

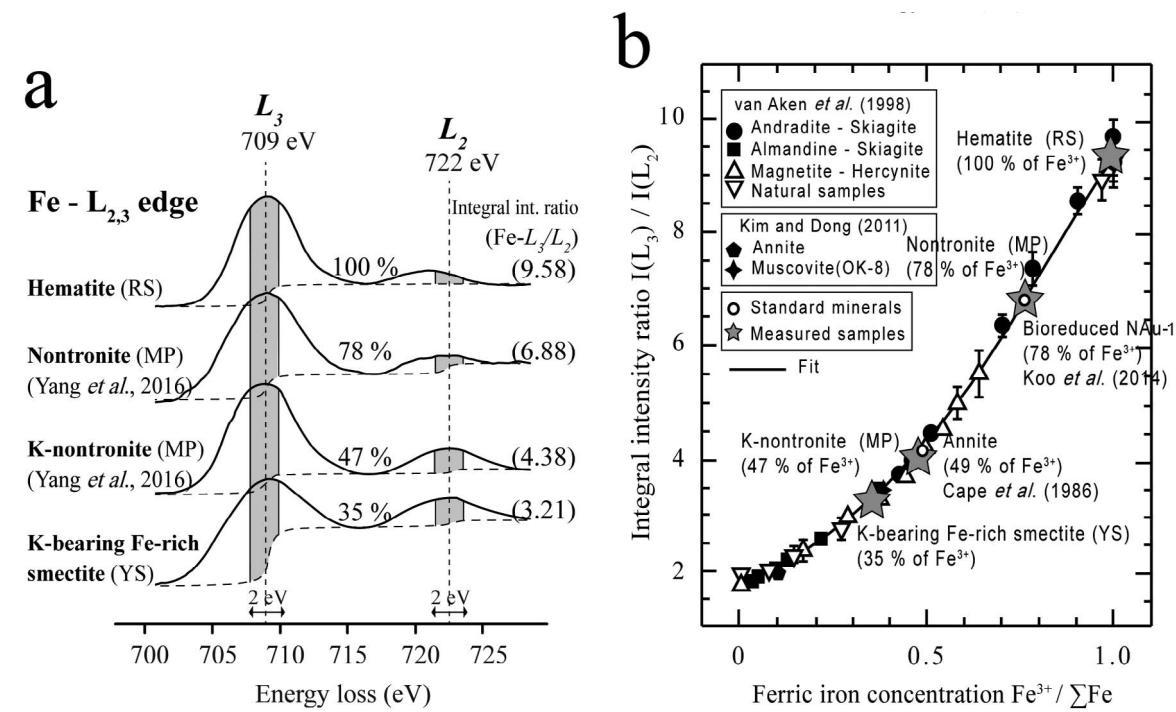

Figure 5. Electron energy loss spectroscopy (EELS) spectra of the Fe-$L_{2,3}$ edges for a) the K-bearing collapsed Fe-rich smectite in the yellow altered sediments (YS), hematite in RS compared to K-nontronite in metalliferous pelagic (MP) sediments (Yang *et al*., 2016), and nontronite in MP (Yang *et al*., 2016). Quantification of the Fe(III) redox state b) was achieved by plotting the integral Fe-$L_{2,3}$ intensity ratios on the universal curves (van Aken *et al*., 1998) for Fe-L_3 (709 eV) and Fe-L_2 (722 eV).

https://doi.org/10.1346/CCMN.2018.064083 Published online by Cambridge University Press

smectites (*e.g.*, palagonite and [proto-]smectite) that originate from the oxidative weathering of basalt (Clayton and Pearce, 2000; Cuadros *et al*., 2011) were reported as dioctahedral nontronites. By considering the increase in the net negative charge of nontronite that was induced by the increased amount of ferrous Fe, observing K-fixation in the interlayers to balance the charge was not surprising. The K was likely supplied from seawater (Clayton and Pearce, 2000). Nonetheless, how the oxidation states of Fe vary in the SPG basaltic basement, which was persistently exposed to oxidizing conditions (D'Hondt *et al*., 2015), was puzzling. The association between microbes and Fe reduction in smectite structures cannot be excluded to explain the variation in Fe-redox states. Previous studies (Koo *et al*., 2014, 2016) indicated that the K-fixation rate has a strong positive relationship with microbial Fe respiration and results in a K-fixed nontronite. Microbially induced K-fixation in nontronite has also been reported as an irreversible reaction. This contrasts with the reversible abiotic reaction (Lee *et al*., 2006; Koo *et al*., 2014) and might explain the reduced Fe form identified in smectite structures under oxidative conditions (D'Hondt *et al*., 2015). Microbial habitats in basalt and deep sub-seafloor sediments have been reported (Fisk *et al*., 2003; D'Hondt *et al*., 2015), which suggests the possibility of a biogeochemical redox reaction.

The observations described above are significant because Fe is an essential nutrient for microorganisms (Johnson *et al*., 1999) in the marine environment. In the formation of K-nontronite, excess Si and highly mobile Fe(II) (Vorhies and Gaines, 2009) can be released because an Fe-rich nontronite has a low Al/Si ratio (0.11) in comparison to a K-bearing nontronite (0.2). Regardless of whether the transformation is biotic or abiotic (Kim *et al*., 2004; Koo *et al*., 2014), a K-bearing Fe-rich smectite formed as a secondary product during basalt alteration is, therefore, a possible new pathway for clay minerals to develop from Fe and Si sources in marine environments. Moreover, the constituents of a nanosize, poorly ordered feroxyhyte (Figure 4a) are more bioavailable in comparison to those from a well ordered hematite, which has a low solubility (Jang *et al*., 2007). This suggests that basalt alteration and the precipitation of secondary mineral phases affects Fe cycling in the sub-seafloor sediments of the SPG.

ACKNOWLEDGMENTS

The authors thank the scientific parties involved in IODP expedition 329 for their indispensable discussions and comments. The present research was supported by a National Research Foundation of Korea (NRF) grant funded by the Korean government (MSIP; No. NRF-2015R1A2A2A01003797) to Jinwook Kim, and the 'International Ocean Discovery Program' funded by the Ministry of Oceans and Fisheries, Korea. TEM analyses were supported by a Korea Basic Science Institute (KBSI) project (T35520).

REFERENCES

Alt, J.C. (1995) Subseafloor processes in mid-ocean ridge hydrothermal systems. Pp. 85–114 in: *Seafloor Hydrothermal Systems: Physical, Chemical, Biological, and Geological Interactions*, (S.E. Humphris, R.A. Zierenberg, L.S. Mulineaux, and R.E. Thomson, editors), American Geophysical Union Geophysical Monograph Series, Vol. 91, DOI: 10.1029/GM091.

Alt, J.C. (2009) Very low-grade hydrothermal metamorphism of basic igneous rocks. Pp. 169–201 in: *Low-grade Metamorphism* (M. Frey and D. Roinson, editors), Blackwell Publishing Ltd., Oxford, UK. DOI: 10.1002/9781444313345.ch6.

Bach, W. and Edwards, K.J. (2003) Iron and sulfide oxidation within the basaltic ocean crust: Implications for chemolithoauthotrophic microbial biomass production. *Geochimica et Cosmochimica Acta*, **67**, 3871–3887.

Bass, M.N. (1976) Secondary minerals in oceanic basalt, with special reference to Leg 34, Deep Sea Drilling Project. in: *Initial Reports of Deep Sea Drilling Project* **34**, 393–432. U.S. Government Printing Office.

Claustre, H. and Maritorena, S. (2003) The many shades of ocean blue. *Science*, **302**, 1514–1515.

Clayton, T. and Pearce, R. (2000) Alteration mineralogy of Cretaceous basalt from ODP site 1001, Leg 165 (Caribbean Sea). *Clay Minerals*, **35**, 719–733.

Cornell, R.M. and Schwertmann, U. (2003) Solubility. Chapter 9, pp. 201–220 in: *The Iron Oxides: Structure, Properties, Reactions, Occurrences and Uses*. John Wiley & Sons, Inc., Hoboken, NJ, USA.

Cuadros, J., Dekov, V.M., Arroyo, X., and Nieto, F. (2011) Smectite formation in submarine hydrothermal sediments: Samples from the HMS Challenger expedition (1872–1876). *Clays and Clay Minerals*, **59**, 147–164.

Cuadros, J., Dekov, V.M., and Fiore, S. (2008) Crystal chemistry of the mixed-layer sequence talc-talc-smectite-smectite from submarine hydrothermal vents. *American Mineralogist*, **93**, 1338–1348.

Cuadros, J., Michalski, J.R., Dekov, V., Bishop, J., Fiore, S., and Dyar, M.D. (2103) Crystal-chemistry of interstratified Mg/Fe-clay minerals from seafloor hydrothermal sites. *Chemical Geology*, **360**, 142–158.

D'Hondt, S., Inagaki, F., and Alvarez Zarikian, C. (2013) IODP expedition 329: Life and habitability beneath the seafloor of the South Pacific Gyre. *Scientific Drilling*, **15**, 4–10.

D'Hondt, S., Spivack, A.J., Pockalny, R., Ferdelman, T.G., Fischer, J.P. Kallmeyer, J., Abrams, L.J., Smith, D.C., Graham, D., and Hasuik, F. (2009) Subseafloor sedimentary life in the South Pacific Gyre. *Proceedings of the National Academy of Sciences*, **106**, 11651–11656.

D'Hondt, S., Inagaki, F., Zarikian, C.A., Abrams, L.J., Dubois, N., Engelhardt, T., Evans, H., Ferdelman, T., Gribsholt, B., Harris, R.N., Hoppie, B.W., Hyun, J.-H., Kallmeyer, J., Kim, J., Lynch, J.E., McKinley, C.C., Mitsunobu, S., Morono, Y., Murray, R.W., Pockalny, R., Sauvage, J., Shimono, T., Shiraishi, F., Smith, D.C., Smith-Duque, C.E., Spivack, A.J., Steinsbu, B.O., Suzuki, Y., Szpak, M., Toffin, L., Uramoto, G., Yamaguchi, Y.T., Zhang, G.-L., Zhang, X.-H., and Ziebis, W. (2015) Presence of oxygen and aerobic communities from sea floor to basement in deep-sea sediments. *Nature Geoscience*, **8**, 299–304.

Dekov, V.M., Cuadros, J., Shanks, W.C., and Koski, R.A. (2008) Deposition of talc-kerolite-smectite-smectite at seafloor hydrothermal vent fields: Evidence from mineralogical, geochemical and oxygen isotope studies. *Chemical Geology*, **247**, 171–194.

Dong, H., Jaisi, D.P., Kim, J., and Zhang, G. (2009) Microbe-

clay mineral interactions. *American Mineralogist*, **94**, 1505–1519.

Edwards, K.J., Bach, W., and McCollom, T.M. (2005) Geomicrobiology in oceanography: Microbe-mineral interactions at and below the seafloor. *Trends in Microbiology*, **13**, 449–456.

Eslinger, E., Highsmith, P., Albers, D., and De Mayo, B. (1979) Role of iron reduction in the conversion of smectite to illite in bentonites in the disturbed belt, Montana. *Clays and Clay Minerals*, **27**, 327–338.

Fisk, M.R., Storrie-Lombardi, M., Douglas, S., Popa, R., McDonald, G., and Di Meo-Savoie, C. (2003) Evidence of biological activity in Hawaiian subsurface basalts. *Geochemistry, Geophysics, Geosystems*, **4**, 1103, DOI:10.1029/2002GC000387.

Gates, W.P., Jaunet, A.-M., Tessier, D., Cole, M.A., Wilkinson, H.T., and Stucki, J.W. (1998) Swelling and texture of iron-bearing smectites reduced by bacteria. *Clays and Clay Minerals*, **46**, 487–497.

Glasauer, S., Weidler, P.G., Langley, S., and Beveridge, T.J. (2003) Controls on Fe reduction and mineral formation by a subsurface bacterium. *Geochimica et Cosmochimica Acta*, **67**, 1277–1288.

Glasby, G.P. (1991) Mineralogy, geochemistry, and origin of Pacific red clays: A review. *New Zealand Journal of Geology and Geophysics*, **34**, 167–176.

Hart, S.R. and Staudigel, H. (1982) The control of alkalies and uranium in seawater by ocean crust alteration. *Earth and Planetary Science Letters*, **58**, 202–212.

Jaisi, D.P., Eberl, D.D., Dong, H., and Kim, J. (2011) The formation of illite from nontronite by mesophilic and thermophilic bacterial reaction. *Clays and Clay Minerals*, **59**, 21–33.

Jang, J.-H., Dempsey, B.A., and Burgos, W.D. (2007) Solubility of hematite revisited: Effects of hydration. *Environmental Science & Technology*, **41**, 7303–7308.

Johnson, K.S., Chavez, F.P., and Friederich, G.E. (1999) Continental-shelf sediment as a primary source of iron for coastal phytoplankton. *Nature*, **398**, 697–700.

Kim, J.-W., Dong, H., Seabaugh, J., Newell, S.W., and Eberl, D.D. (2004) Role of microbes in the smectite-to-illite reaction. *Science*, **303**, 830–832.

Kim, J.-W., Furukawa, Y., Daulton, T.L., Lavoie, D., and Newell, S.W. (2003) Characterization of microbially Fe(III)-reduced nontronite: Environmental cell-transmission electron microscopy study. *Clays and Clay Minerals*, **51**, 382–389.

Kim, J.-W., Peacor, D.R., Tessier, D., and Elsass, F. (1995) A technique for maintaining texture and permanent expansion of smectite interlayers for TEM observations. *Clays and Clay Minerals*, **43**, 51–57.

Knowles, E., Wirth, R., and Templeton, A. (2012) A comparative analysis of potential biosignatures in basalt glass by FIB-TEM. *Chemical Geology*, **330**, 165–175.

Koo, T.-H., Jang, Y.-N., Kogure, T., Kim, J.H., Park, B.C., Sunwoo, D., and Kim, J.-W. (2014) Structural and chemical modification of nontronite associated with microbial Fe(III) reduction: Indicators of "illitization". *Chemical Geology*, **377**, 87–95.

Koo, T.-H., Lee, G., and Kim, J.-W. (2016) Biogeochemical dissolution of nontronite by *Shewanella oneidensis* MR-1: Evidence of biotic illite formation. *Applied Clay Science*, **134**, 13–18.

Lee, K., Kostka, J.E., and Stucki, J.W. (2006) Comparisons of structural Fe reduction in smectites by bacteria and dithionite: An infrared spectroscopic study. *Clays and Clay Minerals*, **54**, 195–208.

Melson, W.G. and Thompson, G. (1973) Glassy abyssal basalts, Atlantic Sea floor near St. Paul's Rocks: Petrography and composition of secondary clay minerals. *Geological Society of America Bulletin*, **84**, 703–716.

Nealson, K.H. and Saffarina, D. (1994) Iron and manganese in anaerobic respiration: Environmental significance, physiology, and regulation. *Annual Reviews in Microbiology*, **48**, 311–343.

Orcutt, B.N., Sylvan, J.B., Knab, N.J., and Edwards, K.J. (2011) Microbial ecology of the dark ocean above, at, and below the seafloor. *Microbiology and Molecular Biology Reviews*, **75**, 361–422.

Orcutt, B.N., Wheat, C.G., Rouxel, O., Hulme, S., and Edwards, K.J. (2013) Oxygen consumption rates in subseafloor basaltic crust derived from a reaction transport model. *Nature Communications*, **4**, 2539.

Pichler, T., Ridley, W.I., and Nelson, E. (1999) Low-temperature alteration of dredged volcanics from the Southern Chile Ridge: Additional information about early stages of seafloor weathering. *Marine Geology*, **159**, 155–177.

Roden, E.E. and Zachara, J.M. (1996) Microbial reduction of crystalline iron (III) oxides: Influence of oxide surface area and potential for cell growth. *Environmental Science & Technology*, **30**, 1618–1628.

Seyfried, W., Shanks, W., and Dibble, W. (1978) Clay mineral formation in DSDP Leg 34 basalt. *Earth and Planetary Science Letters*, **41**, 265–276.

Stucki, J.W., Komadel, P., and Wilkinson, H.T. (1987) Microbial reduction of structural iron (III) in smectites. *Soil Science Society of America Journal*, **51**, 1663–1665.

Stucki, J.W. and Koska, J.E. (2006) Microbial reduction of iron in smectite. *Comptes Rendus Geoscience*, **338**, 468–475.

van Aken, P.A. and Liebscher, B. (2002) Quantification of ferrous/ferric ratios in minerals: New evaluation schemes of Fe L_{23} elecron energy-loss near-edge spectra. *Physics and Chemistry of Minerals*, **29**, 188–200.

van Aken, P.A., Liebscher, B., and Styrsa, V.J. (1998) Quantitative determination of iron oxidation states in minerals using Fe $L_{2,3}$-edge electron energy-loss near-edge structure spectroscopy. *Physics and Chemistry of Minerals*, **25**, 323-327.

Vorhies, J.S. and Gaines, R.R. (2009) Microbial dissolution of clay minerals as a source of iron and silica in marine sediments. *Nature Geoscience*, **2**, 221–225.

Wu, J., Roth, C.B., and Low, P.F. (1988) Biological reduction of structural iron in sodium-nontronite. *Soil Science Society of America Journal*, **52**, 295–296.

Yang, K., Kim, J.-W., Kogure, T., Dong, H., Baik, H., Hoppie, B., and Harris, R. (2016) Smectite, illite, and early diagenesis in South Pacific Gyre subseafloor sediment. *Applied Clay Science*, **134**, 34–43.

Zhang, G., Smith-Duque, C., Tang, S., Li, H., Zarikian, C., D'Hondt, S., Inagaki, F., and IODP Expedition 329 Scientists. (2012) Geochemistry of basalts from IODP site U1365: Implications for magmatism and mantle source signatures of mid-Cretaceous Osbourn Trough. *Lithos*, **144**, 73–87.

(*Received 28 September 2017; revised 11 December 2017; Ms. 1209; AE: R. Zhu*)